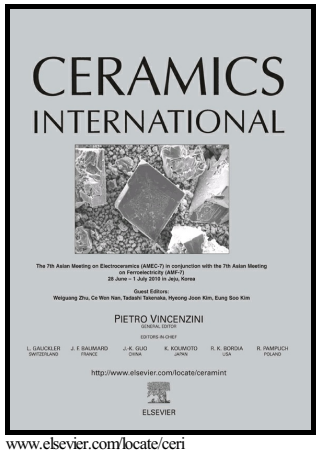

www.elsevier.com/locate/ceri

Effect of *A*-Site Cation Ordering on the Thermoelectric Properties of the Complex Cobalt Oxides $Gd_{1-x}Sr_xCoO_{3-\delta}$ (x = 0.8 and 0.9)

V.A. Dudnikov, Yu.S. Orlov, N.V. Kazak, A.S. Fedorov, L.A. Solov'yov, S.N. Vereshchagin, A.T. Burkov, S.V. Novikov, S.Yu. Gavrilkin, S.G. Ovchinnikov

PII: S0272-8842(18)30591-1
DOI: https://doi.org/10.1016/j.ceramint.2018.03.037
Reference: CERI17674

To appear in: *Ceramics International*

Received date: 20 November 2017
Revised date: 24 February 2018
Accepted date: 5 March 2018

Cite this article as: V.A. Dudnikov, Yu.S. Orlov, N.V. Kazak, A.S. Fedorov, L.A. Solov'yov, S.N. Vereshchagin, A.T. Burkov, S.V. Novikov, S.Yu. Gavrilkin and S.G. Ovchinnikov, Effect of *A*-Site Cation Ordering on the Thermoelectric Properties of the Complex Cobalt Oxides $Gd_{1-x}Sr_xCoO_{3-\delta}$ (x = 0.8 and 0.9), *Ceramics International,* https://doi.org/10.1016/j.ceramint.2018.03.037

Effect of *A*-Site Cation Ordering on the Thermoelectric Properties of the Complex Cobalt Oxides $Gd_{1-x}Sr_xCoO_{3-\delta}$ (x = 0.8 and 0.9)

V.A. Dudnikov[1], Yu.S. Orlov[1,2], N.V. Kazak[1], A.S. Fedorov[1,2], L.A. Solov'yov[3], S.N. Vereshchagin[3], A.T. Burkov[4], S.V. Novikov[4], S.Yu. Gavrilkin[5], and S.G. Ovchinnikov[1,2]

[1]Kirensky Institute of Physics, Federal Research Center KSC SB RAS, Krasnoyarsk, 660036 Russia
[2]Siberian Federal University, Krasnoyarsk, 660041Russia
[3]Institute of Chemistry and Chemical Technology,Federal Research Center KSC SB RAS, Krasnoyarsk, 660049 Russia
[4]Ioffe Physical-Technical Institute, Russian Academy of Sciences, St. Petersburg, 194021 Russia
[5]Lebedev Physical Institute, Russian Academy of Sciences, Moscow, 119991 Russia

Corresponding Author Details: Yu. S. Orlov, Kirensky Institute of Physics KSC SB RAS, 660036 Krasnoyarsk, Russia, Tel: +7(391) 243-26-35, Fax: +7(391) 243-89-23, Email: orlov@iph.krasn.ru, jso.krasn@mail.ru

Abstract

The effect of substitution of Sr^{2+} ions for Gd^{3+} ions on the phase composition, electrical resistivity, thermoelectricity, and thermal conductivity of rare-earth cobalt oxides $Gd_{1-x}Sr_xCoO_{3-\delta}$ (x = 0.8 and 0.9) has been investigated. It has been determined that at the investigated strontium concentrations, the single-phase disordered nonstoichiometric cubic perovskites and superstructures with ordered Sr^{2+}/Gd^{3+} ions and anion vacancies can be formed. The influence of ordering/disordering of *Gd* and *Sr* cations over crystal-lattice *A*- sites on the thermoelectric figure of merit and sample stability at high temperatures has been studied. The thermoelectric figure of merit of the disordered samples was found to exceed by far the analogous parameter of the ordered samples, which allows us to consider the disordering as a way of improving the thermoelectric parameters. Two contributions to the conductivities are discussed: high-temperature thermoactivation and low-temperatures variable range hopping. The parameters of the Mott electronic structure, including DOS $N(\varepsilon_F)$, hopping energy ε (the energy of hopping conductivity activation), and hopping length R_h, have been estimated

Keywords: substituted rare earth cobalt oxides, thermoelectric oxide materials, ordered and disordered states

1. Introduction

The $(A'_{1-x}A''_x)B'_{1-y}B''_yO_z$, compounds, where A' and A'' are lanthanides, rare-earth, or alkali metals and B' and B'' are transition metals, belong to the systems with strong electron correlations, which have been in focus for the past few decades. These materials are interesting for fundamental research and attract close attention by the diversity of possible iso- and heterovalent substitutions and the potential of synthesizing compounds with the desired physicochemical properties for application in various sensors, solid oxide fuel cells, catalysts,

thermoelectric and cathode materials, etc. [1-8] The physical properties of these compounds have been discussed in a great number of experimental and theoretical works [9-16].

A key role in the formation of the properties of $(A'A'')BO_3$ perovskites is played by their crystal and electronic structures and the nature of *A* and *B* cations. In most studies on the interplay of the chemical composition of substituted perovskites and their physical properties, the change in the magnetic behavior or transport properties upon heterovalent substitution in the *A*- site (e.g., Sr^{2+} for La^{3+}) was attributed to the occurrence of oxygen vacancies or the change in the *B*-ion state. The combined electron, X-ray, and neutron diffraction study made it possible to establish the conditions for forming single-phase rare-earth-substituted $Ln_{1-x}Sr_xCoO_{3-\delta}$ ($Ln = La^{3+} – Yb^{3+}$) cobaltites and showed the existence of a complex of tetragonal and orthorhombic superstructures, the properties of which are determined by the cation type and oxygen deficiency [17, 18]. During the $Ln_{1-x}Sr_xCoO_{3-\delta}$ perovskites formation, different equilibrium distributions of Sr^{2+} and Ln^{3+} ions can occur, depending on the ratio between ionic radii of cations. In the elements *Ln = La–Nd*, the structure with the completely disordered distribution of Sr^{2+}/Ln^{3+} cations over crystallographic *A* sites is stable at any temperature [17, 18]. The disordered $Ln_{1-x}Sr_xCoO_{3-\delta}$ perovskites can be obtained in the form of metastable phases by quenching of the high-temperature phases [19]. However, despite a great number of works devoted to the ordered/disordered perovskites, the consideration of the effect of order-disorder transitions on the properties of materials is usually limited to the oxygen vacancy ordering in the anion sublattice, whereas the comparative analysis of physical and chemical properties at different cation distributions over *A*- sites is rarely met [19]. It is worth noting that the ordering of *Gd/Sr* cations leads to the occurrence of specific heat and thermal expansion anomalies and to the extraordinary magnetic behavior near 350 K [20]. Among a huge variety of investigated materials, complex $(A'A'')CoO_{3-\delta}$ cobalt oxides with the perovskite structure hold a special place. They are characterized by the Co^{3+} ion multiplicity fluctuations [21], which lead to the features in the magnetic, electrical, and structural properties [22] and make the physical processes occurring in these compound more difficult to understand. The substituted rare-earth cobaltites can also exhibit intriguing thermoelectric properties. The main characteristic of a thermoelectric material is the thermoelectric conversion efficiency $Z=S^2\sigma/k$, where *S* is the Seebeck coefficient (thermoelectric power), σ is the electrical conductivity, and *k* is the thermal conductivity, which is more frequently determined by the dimensionless thermoelectric figure of merit $ZT = S^2\sigma T/k$ (*T* is the absolute temperature). Thus, the high Seebeck coefficient and electrical conductivity in combination with the low thermal conductivity are the necessary characteristics of a high-quality thermoelectric material. The power factor $P = S^2\sigma$ is determined by the electronic properties of a material, while the thermal conductivity $k = k_{el} + k_{ph}$ is the sum of the electron (k_{el}) and lattice (k_{ph}) contributions. According to the Wiedemann-Franz law, the electrical conductivity and electronic thermal conductivity are related as $k_{el} = L\sigma T$, where *L* is the Lorentz number [23-25]; therefore, the conductivity increases with the electronic thermal conductivity, which complicates the enhancement of the thermoelectric figure of merit. Taking into account that the *ZT* value can be optimized via reducing the phonon thermal conductivity, here we investigated the effects of *A*-site cation ordering/disordering on the thermoelectric and magnetic properties of $Gd_{1-x}Sr_xCoO_{3-\delta}$ (x = 0.8 and 0.9) and perform a comparative analysis of these materials.

2. Experimental

Polycrystalline $Gd_{1-x}Sr_xCoO_{3-\delta}$ (x = 0.8 and 0.9) samples were synthesized from the stoichiometric mixture of Co_3O_4 (99.7%, metals basis), Gd_2O_3 (99.99%, REO), and $SrCO_3$ (99.99%, metals basis) oxides in an alundum crucible using a conventional ceramic technology in the triple grinding-calcination cycle at a temperature of 1473 K for 8 h (24 h in total) in air. The resulting product was thoroughly crushed in an agate mortar and pressed in discs 5 mm in diameter and 1–2 mm in height or in bars 10x5x2 mm in size. Then, the samples were held at 1473 K for 12 hours. One part of the samples was slowly cooled in a furnace in air at a rate of 2 deg/min and the other part of the samples was rapidly cooled (tempered) at a rate of 30 deg/sec. Finally, all the samples were held at 773 K for 6 h to stabilize the oxygen content.

X-ray diffraction study was carried out using a PANalyticalX'PertPRO powder diffractometer (Netherlands, CoKα); images were obtained in a HTK 1200N high-temperature chamber (AntonPaar, Austria) in the 2θ angle range of 10–140 deg. Lattice parameters were determined from the positions of diffraction maxima using the ITO program [26]. The crystal structure was refined by the full profile analysis of X-ray diffraction patterns using the Rietveld method [27] and derivative difference minimization (DDM) [28].

The oxygen content was determined from the mass loss Δm (%) [29] on a NETZSCHSTA449C analyzer equipped with an AeolosQMS 403C mass spectrometer. The mass loss was measured during sample reduction in the 5-% H_2-Ar mixture flux upon heating to 1127 K at a rate of 10 deg/min, assuming cobalt to be reduced to the metallic state. The reduction was performed in a corundum (Al_2O_3) crucible with a perforated cover; the sample mass was 22±0.5 mg. To take into account the ejection force, we performed control measurements on an empty crucible (zero line) under the same conditions. The determination error was δ = ± 0.01.

The thermoelectric power and thermal conductivity measurements and electrical resistivity determination by a four-probe method at 2–300 K were performed on a PPMS-9 Physical Property Measurement System (QuantumDesign, USA) equipped with special units at the Center of Collective Use of the Lebedev Physical Institute, Russian Academy of Sciences.

Temperature dependences of the Seebeck coefficient and electrical resistivity in the temperature range of 300–700 K were obtained on a thermopower and resistivity measurement setup [30] at the Ioffe Physical-Technical Institute, Russian Academy of Sciences.

The discrepancy between the electrical conductivity data obtained by the four-probe method and the thermopower values obtained on a PPMS-9 facility and a thermopower and resistivity measurement setup at the same temperature (300 K) was no higher than 20 % for all the samples.

3. Results and discussion

Gadolinium-strontium cobaltite $Gd_{1-x}Sr_xCoO_{3-\delta}$ (x = 0.8 and 0.9) samples were subjected to heat treatment in different regimes and had the identical chemical composition pairwise, but different distributions of Sr^{2+}/Gd^{3+} cations and anion vacancies over crystal lattice sites (Fig. 1). The samples heated to 1473 K in air represent a cubic perovskite phase with the uniform random distribution of Sr^{2+}/Gd^{3+} cations and anion vacancies over the corresponding crystal lattice sites. Upon rapid (over 30 deg/sec) cooling from 1473 K, the uniform random

distribution of Sr^{2+}/Gd^{3+} ions over the crystal lattice is frozen with the formation of a single-phase metastable material with a cubic structure ($Gd_{1-x}Sr_xCoO_{3-\delta}$-disordered). Upon slow (2 deg/min) cooling from 1473 K to room temperature, the lower-symmetry phase forms due to the partial ordering of Sr^{2+}/Gd^{3+} cations and anion vacancies, as indicated by the occurrence of additional superstructural reflections ($Gd_{1-x}Sr_xCoO_{3-\delta}$-ordered). The tetragonal cation/vacancies ordered phase formed was similar to that described in [31] for $Ln_{1-x}Sr_xCoO_{3-\delta}$ and the process of Sr^{2+}/Gd^{3+} cation ordering was studied by us in detail earlier [32]. The phase purity of tetragonal perovskite was confirmed by precise XRD structural analysis and complete crystal structures of the tetragonal ordered perovskites were refined using the DDM method [28] that has been proven to provide detailed and reliable structural information from powder diffraction data including the atomic coordinates and site occupancies. The method applied did not reveal in the annealed samples any phase but tetragonal ordered perovskite. X-ray diffraction patterns of the $Gd_{1-x}Sr_xCoO_{3-\delta}$ (x = 0.8 and 0.9) samples with the ordered and disordered *Sr/Gd* distribution are shown in Fig. 2. The main properties of the samples are given in Table 1. For all the investigated $Gd_{1-x}Sr_xCoO_{3-\delta}$ (x = 0.8 and 0.9) cobaltites, the δ value of the ordered samples is larger.

Figure 3 shows temperature dependences of the resistivity for the synthesized samples, which exhibit a semiconductor character. Temperature dependences of the resistivity in the heating/cooling regimes are fully identical. At temperatures below 100 K, the resistivity of the ordered samples at fixed temperatures is much higher than that of the disordered ones. This property is observed up to room temperature, at which this difference becomes smaller, although remains over the entire temperature range (Inserts in Figs. 3a and 3b). Comparison of the samples with different substitution levels shows that at the same ordering/disordering the resistivity of the compounds with x = 0.1 is smaller than that of the compounds with x = 0.2.

Figure 3 presents the temperature dependence of the resistivity. The higher resistivity of the ordered samples can be attributed to the unit cell symmetry lowering at the transition from the cubic to tetragonal lattice structure of the perovskite, which results from the partial ordering of Sr^{2+}/Gd^{3+} cations and anion vacancies. The similar increase in the resistivity (the electrical conductivity drop) with the symmetry lowering from cubic to orthorhombic was observed in undoped $LnCoO_3$ rare-earth cobaltites (*Ln* – lanthanide) with a decrease in the average ionic radius [33] (upon isovalent substitution of one rare-earth ion for another [34]), which is accompanied by a decrease in the *Co-O-Co* bond angles from 180̊ and overlap of 3*d* Co^{3+} and 2*p* O^{2-} orbitals in the CoO_6 octahedron [35, 36]. The ordered samples had the larger number of oxygen vacancies (over δ) than the disordered ones at the same sintering condition, which results in the lower carrier density (the lower conductivities). In addition, the higher oxygen vacancy concentration can lead to an increase in the *Co–O* bond length and *O–Co–O* bond angle from the ideal 180° bond angle, which causes a decrease in the overlap between the 3*d Co* and 2*p O* orbitals and band widths.

In spite of the fact that the tetragonal phase has an ordered structure, nevertheless, there is some disorder in the system which is due to the not rigidly fixed but more or less preferable arrangement of ions in the crystal lattice sites. This leads to the appearance of tails of the density of states of the valence band and the conduction band and the edges of mobility

[37] E_{v_1} and E_{v_2} (Fig. 4a). The width of the band gap is defined as $E_g^{(ord)} = E_{v_1} - E_{v_2}$. In the cubic phase there is total disorder which also leads to the appearance of localized states in the spectrum. Since a semiconducting resistance course is observed for disordered cubic samples at low temperatures, they can be attributed to the intermediate-doped case, when the impurity band is separated by forbidden regions from both the valence band and the conduction band or by the region of localized states (Fig. 4b). Since the electrical resistivity of ordered samples at low temperatures exceeds the electrical resistivity of disordered ones, we should expect that $E_g^{(ord)} > E_g^{(dis)}$.

At the sufficiently high temperatures (T > 200 K), the resistivity of all the samples exhibits the thermoactivated behavior $ln(\rho) = A_{act} \cdot (E_a/k_BT)$ (inset in Fig. 3). The fitting parameters for the high-temperature range are given in Table 2. The activation energy E_a is about 0.05–0.1 eV; the value for the ordered samples is higher. As the temperature decreases, the resistivity increasingly deviates from the linear law, i.e., does not agree with the data of this model. The dependence of $ln(\rho)$ on $T^{-1/4}$ (Fig. 5) shows the variable range hopping (VRH) behavior of all the compounds. The general hopping conductivity expression is $\rho(T) = A_{VRH} \cdot exp(T_0/T)^{1/4}$. Here, T_0 – is the Mott conductivity characteristic temperature $T_0 = \frac{B}{k_B N(\varepsilon_F) \zeta^3}$, where $N(\varepsilon_F)$ – is the density of states (DOS) at the Fermi level, ξ is the localization length, B=21 is the constant, and k_B is Boltzmann constant [38]. Ignoring the temperature dependence of pre-factor A_{VRH}, we fitted the low-temperature resistivity data and found that the linear correlation coefficient R rises in the VRH regime, which strongly supports the investigated model. For example, for the ordered $Gd_{0.2}Sr_{0.8}CoO_{3-\delta}$ sample, a straight fitting these curves yields R = 0.9887 for the activated mode and R = 0.9997 for the VRH mode. Assuming the carrier wave function to decay with a decrease in distance r as $\varphi \sim exp(-r/\xi)$, the Mott VRH works when the hopping length exceeds the localization radius ($R_h > \xi$). The Mott electronic structure parameters, including the DOS $N(\varepsilon_F)$, hopping energy ε (the activation energy determining the hopping conductivity), and hopping length R_h, were estimated at temperatures of T = 65 for $Gd_{0.1}Sr_{0.9}CoO_{3-\delta}$ and T = 87 K for $Gd_{0.2}Sr_{0.8}CoO_{3-\delta}$ as $R_h = \frac{3}{8}\xi\left(\frac{T_0}{T}\right)^{\frac{1}{4}}$, $\varepsilon = \frac{3}{4\pi R_h^3 N(\varepsilon_F)}$, where the localization length ξ was taken equal to the Bohr radius r_0 = 3 Å. The $N(\varepsilon_F)$ values are about 10^{20}–10^{21}, which is typical of conventional oxides (Table 3). The energy required for carrier transport between two localized states with different ε values was found to be ~0.01 eV. The carriers moved within the hopping interval R_h, which is larger than the localization length ξ by a factor of almost 10.

Figure 6 shows temperature dependences of the thermal conductivity k (Fig. 6a) and Seebeck coefficient (thermoelectric power) S (Fig. 6b) for the ordered and disordered $Gd_{1-x}Sr_xCoO_{3-\delta}$ samples. With an increase in temperature, the thermoelectric power of all the samples changes its sign from negative to positive, and, for the disordered samples, the transition temperature, as well as the absolute values of maxima, are much higher than those for the ordered compounds. The maximum S value is observed in the disordered $Gd_{0.2}Sr_{0.8}CoO_{3-\delta}$ sample and amounts to 110 μV/K at 235 K; S = 0 at T = 98 K. The higher thermoelectric power of the disordered samples is most likely due to the fact that the mobile oxygen amount in the metastable cubic cobaltites is higher than in the stable tetragonal forms [19].

The thermal conductivity increases with temperature and the $Gd_{0.2}Sr_{0.8}CoO_{3-\delta}$ compounds are characterized by the almost linear monotonic dependences, while the thermal conductivity of $Gd_{0.1}Sr_{0.9}CoO_{3-\delta}$ increases sharply near 175 K.

Figure 7 shows temperature dependences of the electronic thermal conductivity calculated using the Wiedemann-Franz law $k_{el} = L\sigma T$, where $L = 2.44 \times 10^{-8}$ V^2K^{-2} is the Lorentz constant for the degenerate electron statistics [25]. It can be seen that the k_{el} values increase monotonically with increasing temperature and are not large; therefore, the main contribution to the total thermal conductivity in the investigated temperature range is made by the thermal conductivity of the lattice.

Figure 8 shows temperature dependences of the dimensionless thermoelectric figure of merit for the ordered and disordered $Gd_{1-x}Sr_xCoO_{3-\delta}$ samples, which were calculated using the experimental electrical resistivity, thermoelectric power, and thermal conductivity data. In the obtained dependences, the maxima are observed at T = 284 K for the $Gd_{0.2}Sr_{0.8}CoO_{3-\delta}$-disordered compound ($ZT$ = 0.057), at T = 179 K for the $Gd_{0.1}Sr_{0.9}CoO_{3-\delta}$-disordered compound ($ZT$ = 0.006), at T = 300 K for the $Gd_{0.2}Sr_{0.8}CoO_{3-\delta}$-ordered compound ($ZT$ = 0.002), and at T = 248 K for the $Gd_{0.1}Sr_{0.9}CoO_{3-\delta}$-ordered compound ($ZT$ = 0.0005). It can be seen that the maximum figure of merit of the disordered samples significantly exceeds the figure of merit of the ordered samples. The differences by a factor of almost 30 for $Gd_{0.2}Sr_{0.8}CoO_{3-\delta}$ and by a factor of more than 10 for $Gd_{0.1}Sr_{0.9}CoO_{3-\delta}$ are observed. These results allow us to consider fabrication of disordered metastable cubic cobaltites to be a way of improving the thermoelectric figure of merit of such samples.

To estimate the quality of low-temperature data and verify the sample stability in the high-temperature range (T > 300 K), we measured the resistivity and thermopower of the $Gd_{1-x}Sr_xCoO_{3-\delta}$-ordered ($x$ = 0.1 and 0.2) samples in the inert atmosphere (Fig. 9). The measurements were performed in the helium (He-99.99%) atmosphere in the heating and cooling regimes. The difference between the data obtained on different facilities under different conditions in the docking temperature range of 300–318 K lies between 5–20 %, which indicates the good measurement quality. The absence of discrepancies in the behavior of electrical resistivity and thermoelectric power at high temperatures in the heating and cooling regimes speaks about the high stability of the ordered $Gd_{1-x}Sr_xCoO_{3-\delta}$ (x = 0.1 and 0.2) compounds.

4. Conclusions

We synthesized $Gd_{1-x}Sr_xCoO_{3-\delta}$ (x = 0.8 and 0.9) gadolinium-strontium cobaltite samples with the identical chemical composition and different Sr^{2+}/Gd^{3+} cation and anion vacancy distributions over crystal lattice sites: (i) random uniform Sr^{2+}/Gd^{3+} distribution with the formation of a metastable single-phase material with a cubic structure ($Gd_{1-x}Sr_xCoO_{3-\delta}$-disordered) and (ii) partial ordering of Sr^{2+}/Gd^{3+} cations and anion vacancies with the formation of a tetragonal superstructure ($Gd_{1-x}Sr_xCoO_{3-\delta}$-ordered). The resistivity and thermal conductivity of the samples with Sr^{2+}/Gd^{3+} cations disordered over the crystal-lattice A sites are systematically lower than those of the partially ordered samples, while the Seebeck coefficient of the former samples is, vice versa, much higher.

We discussed the two contributions to the conductivities: thermoactivation at high temperatures and variable range hopping at low temperatures.

The maximum thermoelectric figure of merit of the disordered samples exceeds by far the figure of merit of the ordered samples. The *ZT* value for disordered $Gd_{0.2}Sr_{0.8}CoO_{3-\delta}$ is larger than for the ordered sample by a factor of almost 30. The ratio for $Gd_{0.1}Sr_{0.9}CoO_{3-\delta}$ is 12. These results allow us to consider fabrication of the disordered metastable cubic cobaltites as a way of improving the thermoelectric figure of merit in similar compounds. The maximum figure of merit *ZT* = 0.057 obtained for the $Gd_{0.2}Sr_{0.8}CoO_{3-\delta}$ compound at *T* = 284 is good for ceramic samples of this type (the thermoelectric conversion efficiency is $Z = 2 * 10^{-4}$ K^{-1}). The absence of discrepancies between the behavior of electrical resistivity and thermoelectric power in the temperature range of 300–700 K in the heating and cooling regimes is indicative of the high temperature stability of the ordered $Gd_{1-x}Sr_xCoO_{3-\delta}$ (*x* = 0.1 and 0.2) compounds.

Acknowledgments

This work was supported by the Russian Science Foundation, project no. 16-13-00060.

5. References

[1] K. Huang, H.Y. Lee, J.B. Goodenough
Sr- and Ni-Doped $LaCoO_3$ and $LaFeO_3$ Perovskites New Cathode Materials for Solid-Oxide Fuel Cells
J. Electrochem. Soc., 145 (1998), pp. 3220–3227

[2] R. Funahashi, S. Urata
Fabrication and application of an oxide thermoelectric system Int. J. Appl. Ceram. Technol., 4 (2007), pp. 297–307

[3] M.W. Haverkort, Z. Hu, J.C. Cezar, T. Burnus, H. Hartmann, M. Reuther, C. Zobel, T. Lorenz, A. Tanaka, N.B. Brookes, H.H. Hsieh, H.-J. Lin, C.T. Chen, L.H. Tjeng
Spin state transition in $LaCoO_3$ studied using soft x-ray absorption spectroscopy and magnetic circular dichroism
Phys. Rev. Lett., 97 (2006), pp. 176405

[4] C.E. Baumgartner, R.H. Arendt, C.D. Iacovangelo, B.R. Karas
Molten carbonate fuel cell cathode materials study
J. Electrochem. Soc., 131 (1984), pp. 2217–2221

[5] A. Boudghene Stambouli, E. Traversa
Solid oxide fuel cells (SOFCs): a review of an environmentally clean and efficient source of energy
Renewable Sustainable Energy Rev., 6 (2002), pp. 433–455

[6] H. Wang, Z. Zhao, P. Liang, C.M. Xu, A.J. Duan, G.Y. Jiang, J. Xu, J. Liu
Highly active $La_{1-x}K_xCoO_3$ perovskite-type complex oxide catalysts for the simultaneous removal of diesel soot and nitrogen oxides under loose contact conditions
Catal. Lett., 124 (2008), pp. 91–99

[7] P. Tomes, R. Robert, M. Trottmann, L. Bocher, M.H. Aguirre, J. Hejtmanek, A. Weidenkaff

Synthesis and characterization of new ceramic thermoelectrics implemented in a thermoelectric oxide module
J. Electron. Mater., 39 (2010), pp. 1696–1703

[8] A. Weidenkaff, R. Robert, M.H. Aguirre, L. Bocher, T. Lippert, S. Canulescu
Development of thermoelectric oxides for renewable energy conversion technologies
Renewable Energy, 33 (2008), pp. 342–347

[9] I.O. Troyanchuk, A.N. Chobot, A.V. Nikitin, O.S. Mantytskaya, L.S. Lobanovskii, V.M. Dobryanskii
Influence of the oxygen content on the magnetic and transport properties of the $La_{0.45}Ba_{0.55}CoO_{3-x}$ cobaltites
Physics of the Solid State, 57 (2015), pp. 2427–2430

[10] I.O. Troyanchuk, L.S. Lobanovskii, S.V. Dubkov, Yu.I. Shilyaeva, M.V. Silibin, S.A. Gavrilov
Magnetic properties of cobaltites doped with chromium, gallium, and iron ions
Phys. Solid State, 58 (2016), pp. 293–295

[11] T.N. Vasil'chikova, T.G. Kuz'mova, A.A. Kamenev, A.R. Kaul', A.N. Vasil'ev
Spin states of cobalt and the thermodynamics of $Sm_{1-x}Ca_xCoO_{3-\delta}$ solid solutions
JETP Letters, 97 (2013), pp. 34–37

[12] K. Yoshii, S. Tsutsui, A. Nakamura
Magnetic and Structural Properties of $Pr_{1-x}A_xCoO_3$ (A = Sr and Ba)
JMMM, 226 (2001), pp. 829–830

[13] A.A. Kozlovskii, V.F. Khirnyi, A.V. Semenov, V.M. Puzikov
Effect of the spin and valence states of cobalt ions on the kinetic properties of $Ho_{1-x}Sr_xCoO_{3-\delta}$ and $Er_{1-x}Sr_xCoO_{3-\delta}$ compounds
Physics of the Solid State, 53 (2011), pp. 707–716

[14] V.V. Sikolenko, V.V. Efimov, S. Schorr, C. Ritter, I.O. Troyanchuk
Neutron diffraction studies of the structure of substituted complex cobalt oxides
Physics of the Solid State, 56 (2014), pp. 77–80

[15] A.P. Nemudry, O.N. Koroleva, Y.T. Pavlyukhin, O.Y. Podyacheva, Z.R. Ismagilov
Synthesis and Study of Physicochemical Properties of Perovskites Based on Strontium Cobaltite
Bulletin of the Russian Academy of Sciences: Physics, 67 (2003), pp. 1053–1055

[16] N.A. Babushkina, A.N. Taldenkov, S.V. Strelsov, A.V. Kalinov, T.G. Kuzmova, A.A. Kamenev, A.R. Kaul, D.I. Khomskii, K.I. Kugel
Effect of Eu doping and partial oxygen isotop substitution on magnetic phase transitions in $(Pr_{1-y}Eu_y)_{0,7}Ca_{0,3}CoO_3$ cobaltites
JETP, 118 (2014), pp. 266–278

[17] James, M.; Morales, L.; Wallwork, K.; Avdeev, M.; Withers, R.; Goossens, D.

Structure and magnetism in rare earth strontium-doped cobaltates
Physica B: Condensed Matter, 385–386 (2006), pp. 199-201

[18] M. James, T. Tedesco, D.J. Cassidy, R.L. Withers
Oxygen vacancy ordering in strontium doped rare earth cobaltate perovskites $Ln_{1-x}Sr_xCoO_{3-\delta}$ (Ln = La, Pr and Nd; x > 0.60)
Materials Research Bulletin, 40 (2005), pp. 990–1000

[19] S.N. Vereshchagin, L.A. Solovyov, E.V. Rabchevskii, V.A. Dudnikov, S.G. Ovchinnikov, A.G. Anshits
Methane oxidation over A-site ordered and disordered $Sr_{0.8}Gd_{0.2}CoO_{3-\delta}$ perovskites
Chemical Communications, 50 (2014), pp. 6112–6115

[20] V.A. Dudnikov, Yu.S. Orlov, S.Yu. Gavrilkin, M.V. Gorev, S.N. Vereshchagin, L.A. Solov'yov, N.S. Perov, S.G. Ovchinnikov
Effect of Gd and Sr Ordering in A Sites of Doped $Gd_{0.2}Sr_{0.8}CoO_{3-\delta}$ Perovskite on Its Structural, Magnetic, and Thermodynamic Properties
J. Phys. Chem. C, 120 (2016), pp. 13443–13449

[21] S.V. Vonsovskii, M.S. Svirskii
The Effect of the Multiplicity of d (f) Shells on Electron Interaction in Crystals
Sov. Phys. JETP, 20 (1965), pp. 914–921

[22] N.B. Ivanova, S.G. Ovchinnikov, M.M. Korshunov, I.M. Eremin, N.V. Kazak
Specific features of spin, charge, and orbital ordering in cobaltites
Phys. Usp., 52 (2009), pp. 789–810

[23] J.R. Drabble and H.J. Goldsmid
in International Series of Monographs on Semiconductors 4, Thermal Conduction in Semiconductors, edited by H.K. Henisch
Pergamon Press, Oxford (1961)

[24] J.-W. Moon, W.-S. Seo, H. Okabe, T. Okawa, K. Koumoto
Ca-doped $RCoO_3$ (R= Gd, Sm, Nd, Pr) as thermoelectric materials
J. Mater. Chem., 10 (2000), pp. 2007–2009

[25] A.V. Dmitriev, I.P. Zvyagin
Current trends in the physics of thermoelectric materials
Physics-Uspekhi, 53 (2010), pp. 789–803

[26] J.W. Visser
A Fully Automatic Program for Finding the Unit Cell from Powder Data
J. Appl. Crystallogr., 2 (1969), pp. 89−95

[27] H.M. Rietveld
A Profile Refinement Method for Nuclear and Magnetic Structures
J. Appl. Crystallogr., 2 (1969), pp. 65−71

[28] L.A. Solov'yov
Full-Profile Refinement by Derivative Difference Minimization
J. Appl. Crystallogr., 37 (2004), pp. 743−749

[29] K. Conder, E. Pomjakushina, A. Soldatov, E. Mitberg
Oxygen content determination in perovskite-type cobaltates
Materials Research Bulletin, 40 (2005), pp. 257–263

[30] A.T. Burkov, A. Heinrich, P.P. Konstantinov, T. Nakama, K. Yagasaki,
Experimental set-up for thermopower and resistivity measurements at 100-1300 K
Meas. Sci. Technol., 12 (2001), pp. 264–272

[31] M. James, D. Cassidy, D.J. Goossens, R.L. Withers
The phase diagram and tetragonal superstructures of the rare earth cobaltate phases $Ln_{1-x}Sr_xCoO_{3-\delta}$ (Ln=La^{3+}, Pr^{3+}, Nd^{3+}, Sm^{3+}, Gd^{3+}, Y^{3+}, Ho^{3+}, Dy^{3+}, Er^{3+}, Tm^{3+} and Yb^{3+})
J. Solid State Chem., 177 (2004), pp. 1886–1895

[32] S. Vereshchagin, V. Dudnikov, N. Shishkina, L. Solovyov
Phase transformation behavior of $Sr_{0.8}Gd_{0.2}CoO_{3-\delta}$ perovskite in the vicinity of order-disorder transition
Thermochimica Acta, 655 (2017), pp. 34–41

[33] J.A. Alonso, M.J. Martınez-Lope, C. de la Calle, V. Pomjakushin
Preparation and structural study from neutron diffraction data of $RCoO_3$ (R = Pr, Tb, Dy, Ho, Er, Tm, Yb, Lu) perovskites
J. Mater. Chem., 16 (2006), pp. 1555–1560

[34] H. Hashimoto, T. Kusunosec, T. Sekino
Thermoelectrics properties of perovskite-type rare earth cobalt oxide solid solutions $Pr_{1-x}Dy_xCoO_3$
J. of Ceramic Processing Research, 12 (2011), pp. 223–227

[35] J.B. Torrance, P. Lacorre, A.I. Nazzal, E.J. Ansaldo, Ch. Niedermayer
Systematic study of insulator-metal transitions in perovskites $RNiO_3$ (R = Pr, Nd, Sm, Eu) due to closing of charge-transfer gap
Phys. Rev. B, 45 (1992), pp. 8209–8212

[36] T. Arima, Y. Tokura, J.B. Torrance
Variation of optical gaps in perovskite-type 3d transition-metal oxides
Phys. Rev. B, 48 (1993), pp. 17006–1700

[37] I.M. Lifshitz
Energy spectrum structure and quantum states of disordered condensed systems
Sov. Phys. Usp., 7 (1965), pp. 549–573

[38] B.I. Shklovskii, A.L. Efros
Electronic Properties of Doped Semiconductors

Springer-Verlag, Berlin, (1984)

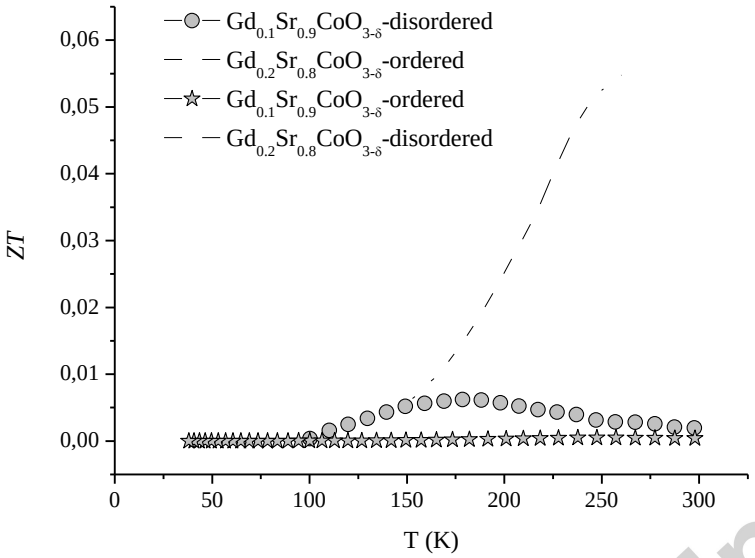

TOC: Temperature dependences of the dimensionless thermoelectric figure of merit of the ordered (stars) and disordered (circles) $Gd_{1-x}Sr_xCoO_{3-\delta}$ samples.

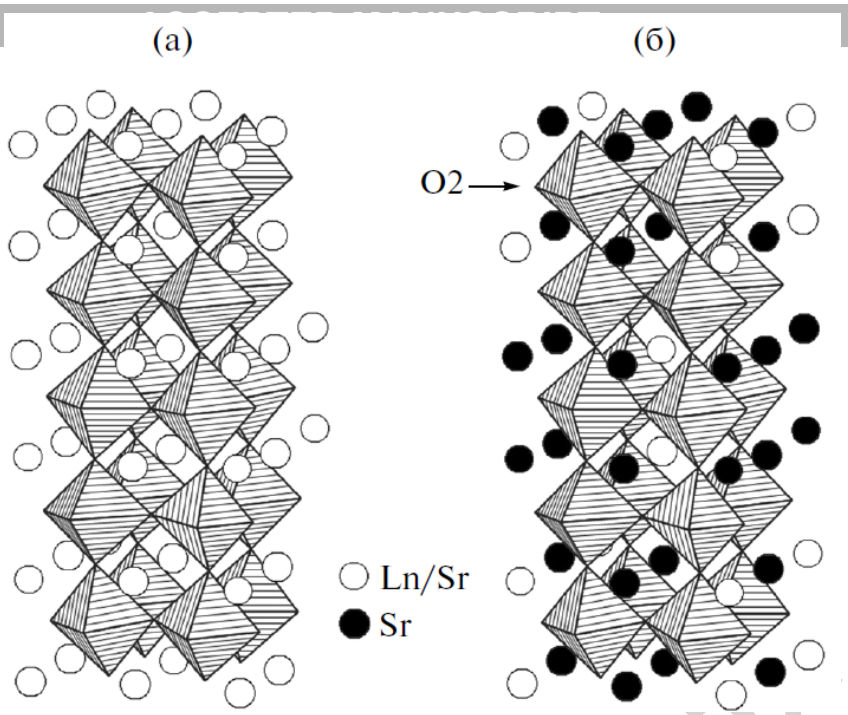

Fig. 1. Schematic of (a) the ideal cubic structure and (b) the structure ordered over the A sitesof the $Ln_{1-x}Sr_xCoO_{3-\delta}$ (*Ln = Sm, Gd, Dy, Y, Ho, Er, Tm, Yb*) double perovskite [31]. White and black circles indicate A sites and octahedra show B-cation positions. Oxygen ions/anion vacancies are located at the octahedra apexes. O2 marks the primary oxygen vacancy localization in the ordered structure.

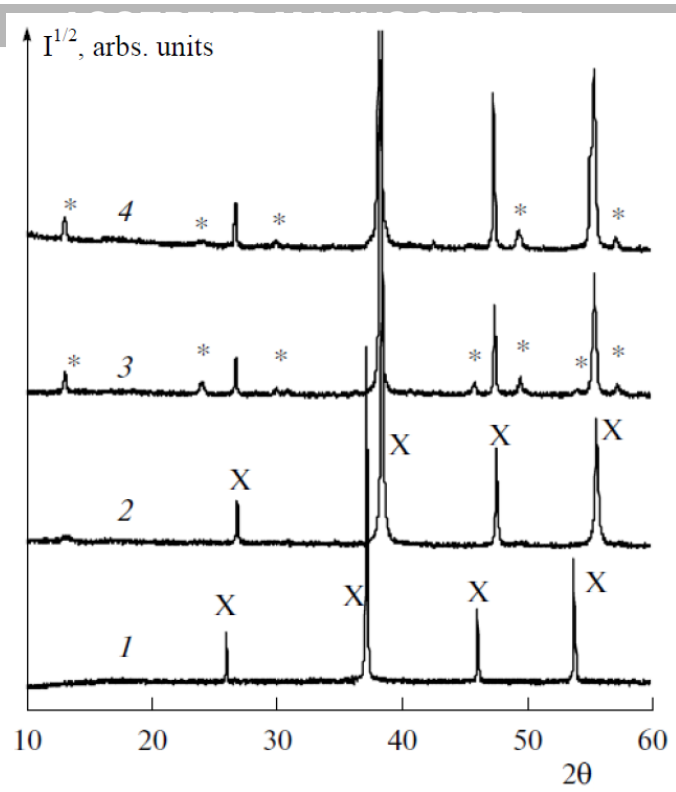

Fig. 2. X-ray diffraction patterns of (1) $Gd_{0.2}Sr_{0.8}CoO_{3-\delta}$ at T = 1473 K, (2) $Gd_{0.2}Sr_{0.8}CoO_{3-\delta}$-disordered at T = 298 K, (3) $Gd_{0.2}Sr_{0.8}CoO_{3-\delta}$-ordered at T = 298 K, and (4) $Gd_{0.1}Sr_{0.9}CoO_{3-\delta}$-ordered at T = 298 K. X is cubic perovskite structure reflections and * is the superstructural reflections of the tetragonal perovskite.

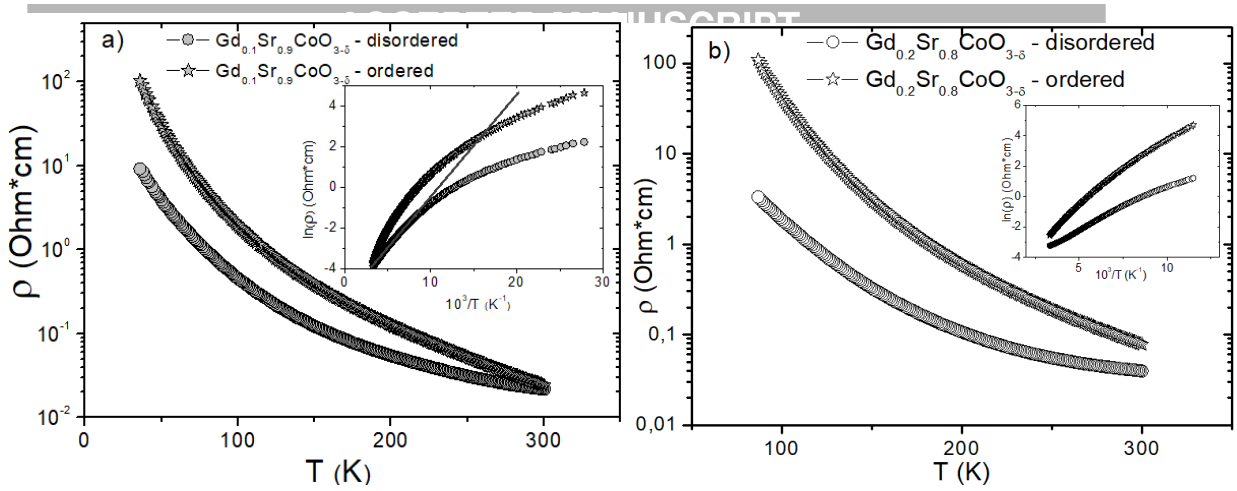

Fig. 3. Temperature dependences of the cobaltite resistivity. Insets: resistivity data plotted as *ln(ρ)* versus $10^3/T$. The straight line shows the activated behavior of $Gd_{0.1}Sr_{0.9}CoO_{3-\delta}$ at high temperatures.

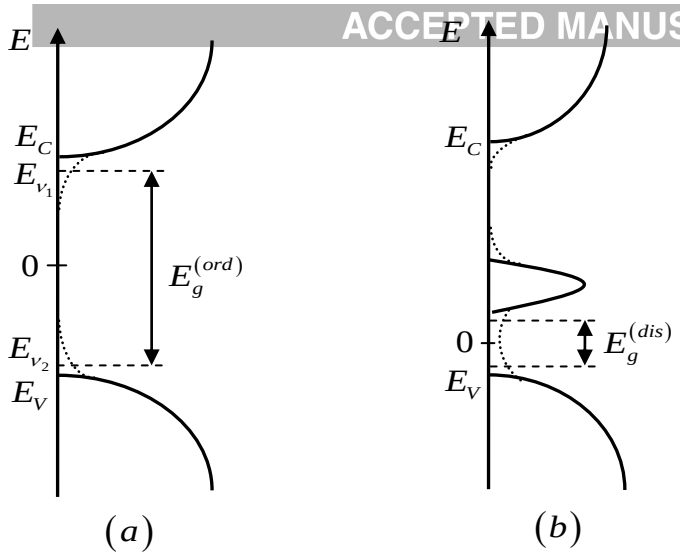

Fig. 4. Scheme of the density of states of tetragonal ordered (a) and cubic disordered (b) perovskites $Gd_{1-x}Sr_xCoO_3$, x = 0.8, 0.9. The valence band, the conduction band, and the impurity band are shown by a solid line. The dotted line shows the tails of the density of states, and the dashed line marks the edges of mobility.

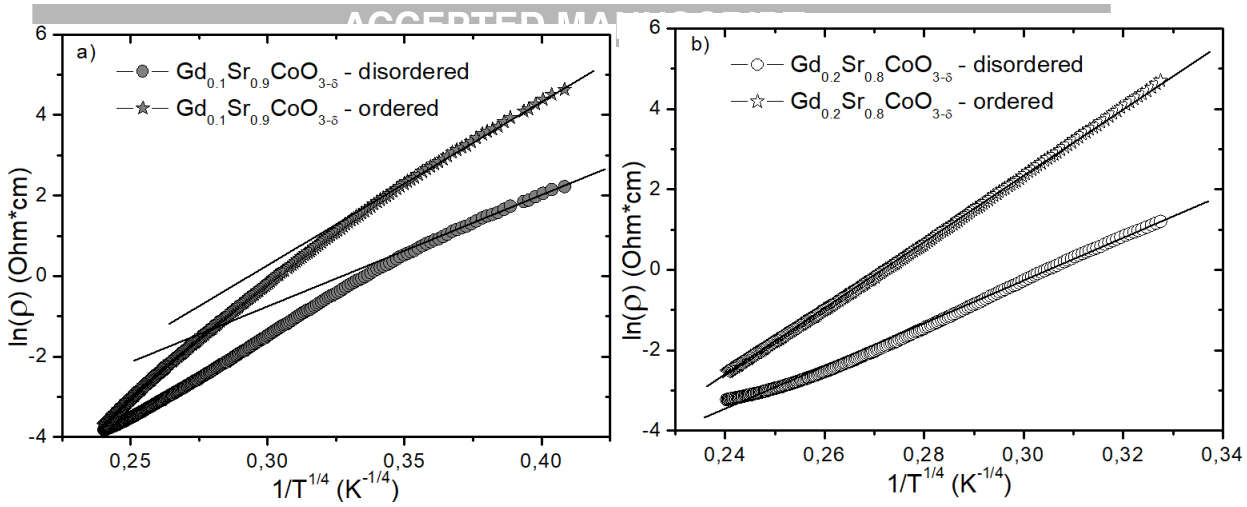

Fig. 5. Dependence of the resistivity on $1/T^{1/4}$. It can be seen that the variable range hopping model fits well the obtained data. The straight lines are linear fits. The fitted parameters are given in Table 1.

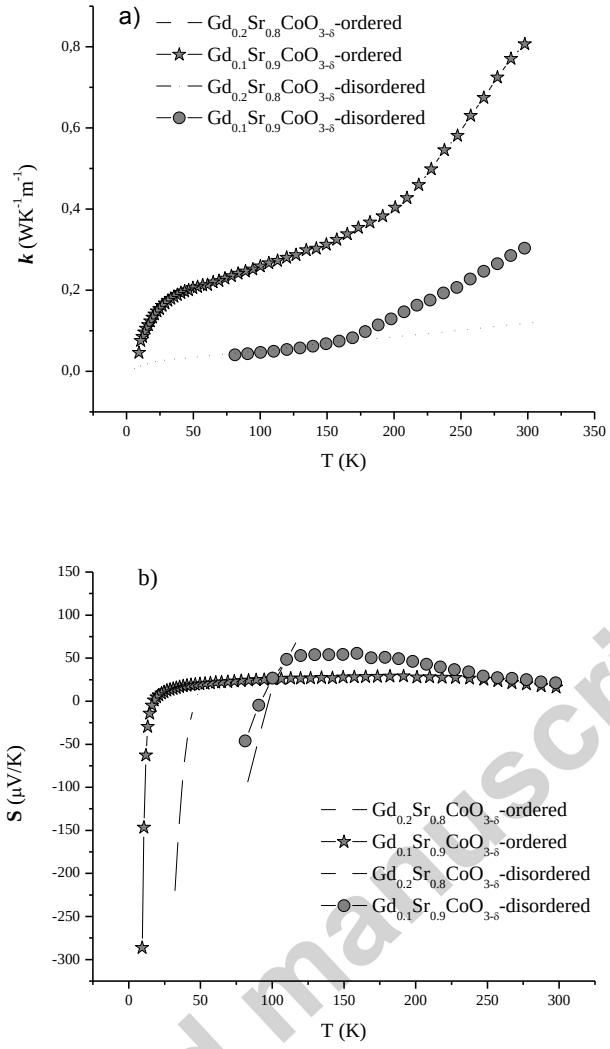

Fig. 6. Temperature dependences of (a) the thermal conductivity and (b) Seebeck coefficient for the ordered (stars) and disordered (circles) $Gd_{1-x}Sr_xCoO_{3-\delta}$ samples.

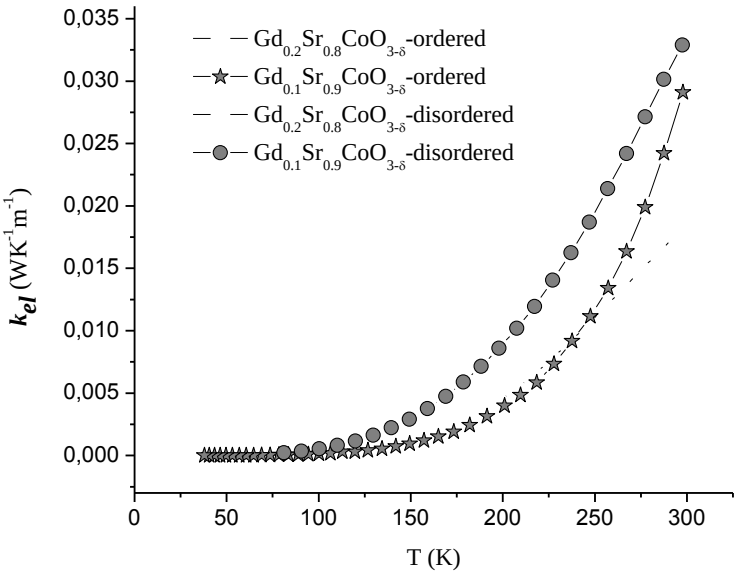

Fig. 7. Temperature dependences of the electronic thermal conductivity for ordered (stars) and disordered (circles) samples $Gd_{1-x}Sr_xCoO_{3-\delta}$.

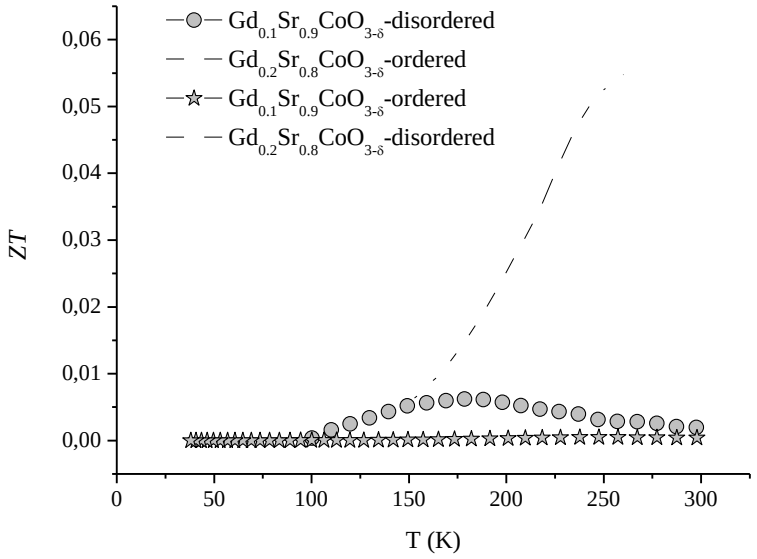

Fig. 8. Temperature dependences of the dimensionless thermoelectric figure of merit of the ordered (stars) and disordered (circles) $Gd_{1-x}Sr_xCoO_{3-\delta}$ samples.

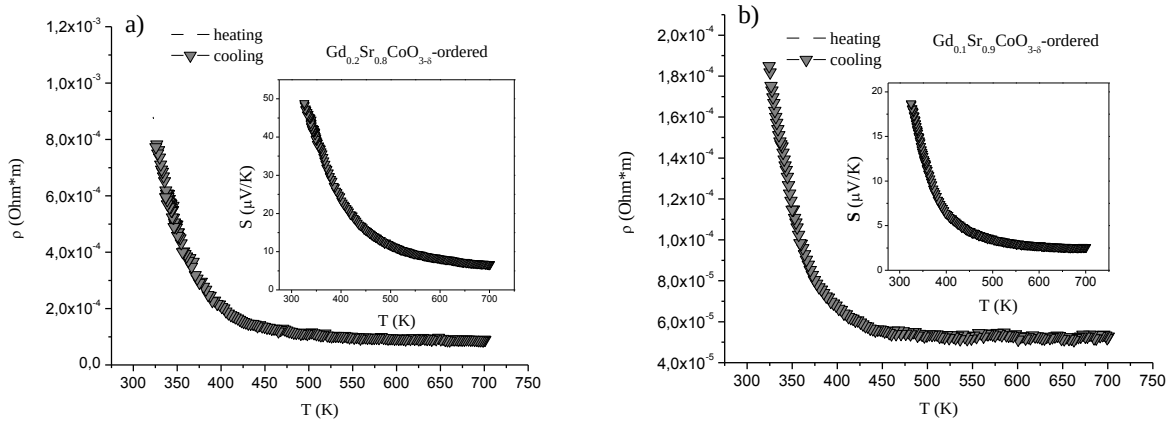

Fig. 9. Temperature dependences of the resistance of (a) the ordered $Gd_{0.2}Sr_{0.8}CoO_{3-\delta}$ and (b) $Gd_{0.1}Sr_{0.9}CoO_{3-\delta}$ samples in the heating (light triangles) and cooling (dark triangles) regimes. Inserts: similar data on the thermoelectric power.

Table 1. Structure, nonstoichiometry (δ) (298 K), and disordering temperatures ($T_{ord\text{-}dis}$) of the $Gd_{1-x}Sr_xCoO_{3-\delta}$ samples

x	δ	State	Lattice	a, Å	b, Å	c, Å	$T_{ord\text{-}dis}$, K
0.2	0.29	disordered	cubic	3.8342 (6)			
0.2	0.37	ordered	tetragonal	7.6785(2)		15.3981 (5)	1383
0.1	0.31	disordered	cubic	3.8462			
0.1	0.33	ordered	tetragonal	3.8428		7.7203	~1263

Table 2. Fitting parameters for the thermoactivated and VRH conductivities

	Thermoactivated regime (200 < T < 300 K)		VRH regime (T < 160 K)	
	$A_{act}\cdot10^{-3}$ (Ω·cm)	E_a (eV)	A_{VRH}(Ω·cm)	$T_0\cdot10^6$ (K)
$Gd_{0.1}Sr_{0.9}CoO_{3-\delta}$-disordered	3.27±0.02	0.049±0.001	$(55.56\pm5.64)\cdot10^{-6}$	0.77±0.03
$Gd_{0.1}Sr_{0.9}CoO_{3-\delta}$-ordered	0.93±0.03	0.086±0.001	$(6.78\pm0.66)\cdot10^{-6}$	2.74±0.07
$Gd_{0.2}Sr_{0.8}CoO_{3-\delta}$-disordered	5.23±0.08	0.051±0.001	$(3.08\pm0.19)\cdot10^{-8}$	10.33±0.15
$Gd_{0.2}Sr_{0.8}CoO_{3-\delta}$-ordered	1.38±0.03	0.106±0.001	$(0.16\pm0.08)\cdot10^{-9}$	47.38±5.52

Table 3. Low-temperature Mott parameters DOS $N(\varepsilon_F)$, hopping energies ε, and hopping lengths R_h for $Gd_{0.1}Sr_{0.9}CoO_{3-\delta}$ (at 65 K) and $Gd_{0.2}Sr_{0.8}CoO_{3-\delta}$ (at 87 K) for a localization length of ζ =3 Å

	$N(\varepsilon_F)$ ($ev^{-1}\cdot cm^{-3}$)	ε (eV)	R_h, Å
$Gd_{0.1}Sr_{0.9}CoO_{3-\delta}$-disordered	$11.74\cdot10^{21}$	0.013	11.73
$Gd_{0.1}Sr_{0.9}CoO_{3-\delta}$-ordered	$3.31\cdot10^{21}$	0.017	16.11
$Gd_{0.2}Sr_{0.8}CoO_{3-\delta}$-disordered	$8.74\cdot10^{20}$	0.030	20.88
$Gd_{0.2}Sr_{0.8}CoO_{3-\delta}$-ordered	$1.91\cdot10^{20}$	0.044	30.56